GSA DATA REPOSITORY 2013349

For Moore et al., 2013, *Glacier slip and seismicity induced by surface melt*

1. FIELD SETTING

Tunnels in the crystalline bedrock beneath Engabreen were excavated in the 1980s and 1990s as part of a hydropower project, administered and maintained by a partnership between the national energy company, Statkraft, and the Norwegian Water Resources and Energy Directorate (NVE). The tunnel system intersects the glacier bed at several locations ("intakes", Figs. DR1 and DR2) where basal meltwater is captured and routed to a hydroelectric power generating facility. Additional surface water intakes in an adjacent valley contribute subaerial snow and ice melt during the melt season through Fonndalstunnelen ("F" in Fig. 1 and Fig. DR1A). One tunnel that intersects the glacier bed has been reserved for subglacial research and allows two points of direct access to the bed for deployment of instrumentation (the "research tunnel" in Fig. DR1B). One access point is through a concrete and steel-reinforced "horizontal shaft" (Fig. DR1B and DR2A). The second access is a "vertical shaft" through ~3 m of rock in the ceiling of the tunnel. A concrete footing and heavy steel support structure within the vertical shaft allow instrumentation to be installed flush with ice sliding across an area of relatively smooth bedrock (Fig. DR1B and DR2). When not in use, both access points are barricaded with customized steel barriers. Water pumps and a water heater supply hot water from a subglacial laboratory approximately 70 m away from the access shafts (Fig. DR1B). Hot water is pumped through insulated hoses to the research tunnel, allowing temporary workspace to be melted at the base of the glacier.

Discharge of subglacial water through this tunnel system is continuously monitored by NVE and Statkraft using several automated stations positioned at different points in the tunnels. Water stage is monitored using OTT Orpheus Mini pressure transducers and converted to discharge with local rating curves. Changes in the discharge from the subglacial intake tunnels may be assumed to reflect the supply-induced changes in the hydraulic capacity of the subglacial drainage system.

Ice overlying the research tunnel is approximately 200 m thick, heavily crevassed, and has a surface slope of approximately 10° (Iverson et al., 2007). The glacier surface elevation there is approximately 830 m above sea level (Lappegard et al., 2006). Surface velocity in this area is ~0.2 m/day (Jackson et al., 2005) and measured sliding velocities during spring are typically ~0.1 m/day (Cohen et al., 2005; Iverson et al., 2007). The intensely-foliated metamorphic rocks over which Engabreen slides exhibit local relief in places exceeding 1m due to differential weathering and erosion along foliation and joint trends. The resulting glacier bed has a high and spatially-variable roughness.

2. MATERIALS AND METHODS

From March 13, 2010, to June 8, 2011, numerous instruments were deployed at the base of the glacier in and around the vertical shaft to measure basal water pressure, bed normal stress, basal shear stress, sliding displacement, ice acceleration, seismicity and acoustic emissions (Fig. DR2B-C). Many of these instruments were extracted, tested and either re-deployed or replaced in early May 2011. Mechanical measurements at the bed were recorded from March 18 to June 11, 2010 and from May 8 to June 8, 2011. A cavity was melted at the bed for instrument deployment from March 7-11, 2010 (through the

vertical shaft) and from May 2-8, 2011 (through the horizontal shaft). Instrumental measurements indicate that creep of ice closes these cavities within two to three days.

2.1. Friction panel

The friction panel has been described elsewhere (Cohen et al., 2005; Iverson et al., 2003); we review only key aspects of it here and refer the reader to this prior work for details. The panel consisted of a 0.3 m diameter granite tablet embedded in a stainless steel housing that sat atop seven low-friction thrust bearings, all housed within a steel and delrin plastic frame that positioned the panel surface flush with the glacier bed (Fig. DR2B-C). The low-friction bearings allowed nearly all of the the shear force exerted by the glacier base over the granite tablet to be transferred to two horizontally-mounted load cells (Geokon 4900X) that presssed against the side of the granite tablet's housing. The force on these load cells was converted to shear stress by taking the square root of the sum of the squared horizontal forces and dividing by the surface area of the tablet. In 2010, only one of the two shear load cells was functional, so the reported shear stress in 2010 represents a minimum value. Similar load cells were mounted vertically in two places adjacent to the granite tablet to measure normal force on the bed.

The basal normal stress was originally computed from these measurements by assuming that these vertical load cells measured the effective normal stress plus the water pressure in the thin water film separating the ice from bedrock. However, observations and measurements (discussed in the main text) consistent with a thin layer of unfrozen sediment at the interface indicate that the measured load must have been partitioned between the stress transferred through the thin water film and any particles within the footprint of the load cell cover that supported some of the ice overburden stress. If the surface of the load-cell cover (surface area A_{tot}) is in real contact with particles over an area sA_{tot} and those particles transfer the local effective stress to the load cell, the actual normal stress is $\sigma_n = \sigma_{meas} + sp_w$. The value of s varies in time and space and can be constrained only to lie between zero and the volume fraction of particles $(1 - n)$, where n is the porosity of the sediment layer. The values reported for effective stress in the main text are computed by assuming $s = 0.3$. Two water pressure transducers (Geokon 4500S) attached to the base of the granite tablet measured the fluid pressure independently in water-filled canisters that were connected with basal water through 10 mm diameter porous discs embedded in the granite.

Lappegard and Kohler (2005) investigated the basal hydraulic system in the area of the research tunnel by pumping water through boreholes (see Fig. DR2B) to the glacier bed and measuring the timing and magnitude of changes in water pressure in boreholes and load cells elsewhere on the glacier bed. Among the key results of this work were the identification of seasonally-varying efficiency and connectedness in the basal hydraulic system. During winter and early spring, expansion of the experimental pressure disturbance over the relatively-flat region of the bed surrounding the vertical shaft was slow and incomplete (see their Figs. 3 and 4). This has been interpreted to indicate that the vertical shaft area is typically unconnected or poorly connected to the winter hydraulic system except when water pressure is elevated and sustained over a sufficiently large area of the bed to locally lift the glacier.

2.2. Other basal measurements

Basal sliding displacement was measured with extensometers (Unimeasure HX-PA series) attached to vinyl-covered (2010) or kevlar-sheathed (2011) cables. These cables passed through boreholes or through conduits in the panel frame and were connected to steel or ABS plastic anchors within the basal ice. Four of these extensometer/anchor devices were deployed in 2010 and five in 2011. In most cases, connections to the anchors were lost within 1 day to 5 weeks of deployment. Since deployment in 2010

was in March, none of the anchors yielded clear sliding signals by mid-May. In 2011, only one extensometer recorded displacement after installation, suggesting that the remaining four cables or cable-anchor connections were compromised quickly.

Data from the panel instruments were recorded with Campbell CR10X and CR1000 dataloggers equipped with a Campbell multiplexer and a vibrating wire interface (AVW1) and automatically downloaded to a laptop running Loggernet software. Timestamps were acquired from the dataloggers, which were synchronized periodically with the laptop. During late March 2010 and late May 2011, a sledgehammer equipped with a trigger switch wired to the CR1000 was pounded on the tunnel floor to allow later synchronization between the seismic data recorders and the dataloggers.

In both 2010 and 2011, an acoustic emissions (AE) sensor (Physical Acoustics R151-AST, 150 KHz resonant frequency) was bonded to the base of the upper platen of the panel housing and logged with a dedicated computer system (Physical Acoustics SAMOS system with AEWin software) powered by a wall outlet in the research tunnel. Owing to the relatively long duration of the measurements and high acoustic data acquisition rates, information from discrete emissions only exceeding 40 dB amplitude was recorded and saved, and no waveforms were recorded. The AE system and its components are described further in an earlier paper (Cohen et al., 2006). The sensor deployed in 2010 failed during or shortly after installation, so data are reported only from 2011.

Custom wireless “smart rocks” designed at Iowa State University were installed in both 2010 and 2011 in basal ice within 1.5 meters of the glacier bed. Each smart rock consisted of a low-noise triaxial accelerometer (Bosch Sensortec BMA-180 1g) connected to a microcontroller (Arduino Pro Mini 328) equipped with a low-power XBee wireless radio transmitter. The electronics were powered by lithium batteries and housed within capped, double-walled PVC cylinders. Each finished smart rock was approximately 25 cm long and 10 cm in diameter. Data were transmitted at ~90 Hz through the bed to an XBee gateway receiver (Digi International) equipped with a high-gain dipole antenna. This antenna was connected directly to a PC laptop running a terminal capture program.

The smart-rocks were expected to record any abrupt changes in local basal sliding velocity associated with stick-slip and concomitant seismicity. As shown in Fig. DR5A, no distinct acceleration signals stand out from the accelerometer noise, even during the May 11 event. This finding is consistent with the interpretation that the discrete seismic events recorded by the broadband seismometers were unrelated to nearby basal slip. The accelerometer did, however, record a DC signal indicative of the orientation of its axes relative to the gravitational acceleration. Thus, a low-pass-filtered signal from the accelerometer can be viewed as a tiltmeter record, providing some insight into changes in strain regime in the ice surrounding the accelerometer (Fig. DR5B). During the May 11 event, the accelerometer recorded the temporary suspension of an otherwise steady and slow rotation. This change in rotation rate may be interpreted to represent a tilt signal counterbalancing steady rotation or the passage of strain transients longitudinally through the glacier.

2.3. Seismic measurements

Guralp 3-T broadband seismometers and Reftek RT130 data loggers were installed throughout subglacial tunnel system, including three locations in the research tunnel shown in Fig. DR1B (VS, HS, 001). Each station recorded continuously at 500 Hz during the spring of 2010 and 2011. The seismometers were installed directly on the rock floor of the tunnel (001) or on concrete slabs adjacent to the basal access points (HS and VS) and were individually powered with lead-acid batteries. Data downloaded from the

broadband seismic stations were inspected in raw form and after processing and filtering in the desired frequency bands. Data were converted from raw form to velocity using the instrument response functions appropriate for the Guralp 3T (see detailed instrument documentation on the IRIS PASSCAL website, http://www.passcal.nmt.edu/content/instrumentation/sensors/broadband-sensors/cmg-3t-bb-sensor). All data are now available from the IRIS seismic catalog listing (http://www.iris.edu/SeismiQuery/) for temporary network 3C.

Impulsive events in the 5-40 Hz frequency band were identified with an automated phase-picking algorithm and binned as a function of time. Due to an increase in seismic noise associated with increased discharge in subglacial tunnels (described further below), the threshold for observing an event is higher later in the spring time-series. The increased noise limited detection of smaller events, however hundreds of events were still observed each day. A subset of the picked events was inspected for phase relationships, and in most cases the signals were dominated by retrograde particle motion (recognized by a 90° phase lag between one or both horizontal channels and the vertical channel), consistent with Rayleigh waves (Fig. DR6). Indeed, preliminary locations for 50 of these events are in heavily-crevassed regions of the ice surface.

Ultra-long period (ULP) signals with period longer than 100 seconds were mostly eliminated with standard deconvolution procedures within the design frequency range of the instrument. Weilandt and Forbriger (1999) showed that at periods exceeding 50 seconds, similar broadband instruments recorded primarily ground tilt. Following these authors, Wiens and others (2005) and Genco and Ripepe (2010) verified that ultra-long period excursions recorded in broadband seismometers on volcanoes provided a high-fidelity measure of tilt. We followed these authors in extracting tilt from the ULP response of our broadband seismometers. Raw digital seismic records were initially filtered in a 100-35,000 second passband. As noted by Wiens and others (2005), while this passband is outside the optimal range of the instrument, the instrument's sensitivity to acceleration falls off linearly with frequency making recovery of long period acceleration signals possible. Instrument response files obtained from the IRIS Data Management Center were used to recover the broadband response without additional frequency-domain filtering using SAC (Seismic Analysis Code, available from the PASSCAL instrument center). Corrected ground velocity data were then differentiated to acceleration, which in the sensor's horizontal channels is proportional to tilt (Genco and Ripepe, 2010). For small angles, an acceleration a corresponds to a tilt of $a/\mathbf{g}$, where $\mathbf{g}$ is the gravitational acceleration vector. From the measurements at Engabreen, tilt angles did not exceed about 6 μrad or 0.0003° from the horizontal.

3. SUPPORTING RESULTS

3.1. Ancillary observations from May 11, 2011

During the May 11 meltwater event, the station at HS began to record high-amplitude broadband noise that made further detection of discrete seismic events at that station impossible. A much more subdued increase in noise was also noted in stations 001 and VS, ~4 m and ~6 m away from station HS, respectively. The onset of this noise during the meltwater event coincided with the cessation of enhanced basal sliding at ~06:30 local time. Based on our direct observations of vigorous water flow through seams in the barricaded horizontal shaft door on May 18 and the seismic record from the same time, we infer that this noise was caused by disturbance and partial submergence of station HS by meltwater and entrained sand (Burtin et al., 2008). This correlation is consistent with an interpretation that hydraulic jacking enlarged basal hydraulic passages and allowed water in over-pressurized cavities to establish or escape into a more efficient drainage system, which in this case included the research tunnel.

Prior to the onset of slip, if effective stress at the debris-bed interface was sufficiently high prior to 04:00 on May 11, such a debris layer would have been immobile due to high friction, with basal motion accommodated by sliding of ice across the top of the debris layer. At the onset of meltwater pressurization, jacking in hydraulically-connected areas of the bed shifted shear stress to poorly-connected areas, thereby increasing shear stress on the debris layer. Uplift of the ice also reduced the local effective stress, so the frictional strength of the debris-rock interface at the base of the debris layer was reduced until shear stress was sufficient to induce slip there. The correlation between the end of the slip episode and the second peak in panel shear stress is consistent with termination of frictional slip and re-strengthening of the debris-rock interface during the recovery of water pressure and normal stress.

3.2. Meltwater events of May 16, 2011 and May 15, 2010

The most prominent seismic and hydraulic disturbance at the glacier base in spring 2011 was on the morning of May 11. As discussed in the main text, this event is interpreted to be the result of extensive surface snowmelt driving downward crevasse propagation and release of meltwater to the bed. A second prominent event occurred late in the evening of May 16th and seems to have been triggered by rain rather than directly by snowmelt. The glacier response to these meltwater events was similarly expressed in seismic measurements from multiple broadband stations as well as by the friction panel (Fig. DR7). Whereas the focus in the main text was to present and interpret the events of May 11 when the dataset is richest and most complete, we provide data from the May 16 event here for comparison and to demonstrate that the May 11 event was not unique.

An additional event expressed similarly in the friction panel and seismic data was recorded on May 15 of 2010 (Fig. DR8-9). Similar to the May 11, 2011 event, this event occurred following several days of sustained warming and presumed surface melting. Instrumental coverage at this time, two months after deployment, was sparser than in 2011, but the sequence of events is consistent. Meltwater supply to the bed increased, causing disturbance of the basal hydraulic system measured as large amplitude swings in effective stress, shear stress and water pressure. An ultra-long period tilt-like signal marked the onset of this disturbance and were followed by sustained increase in the discharge from the subglacial intakes (Fig. DR8).

3.3. Physical analysis of the ULP source

Constraints on the ULP seismic source may be provided by estimating the deformation of the bed as a consequence of hydraulic jacking. Consider the idealized case of a hard, bumpy bed with lee cavities sustained with basal water pressure $p_c < p_o$, where p_o is the ice overburden pressure. In the hours before the May 11 event, the basal water pressure was less than 1.6 MPa. Over the course of the event, water pressure at the panel increased to at least 1.8 MPa, approximately equal to p_o. Assuming that the magnitude of eventual pressure increase in the linked cavity system was at least as large as the pressure change in the unconnected system (i.e., near the panel), pressure in the linked cavity system must have risen at least Δp_c = 0.2 MPa. Assume that cavities cover an areal fraction of the bed a_c of 0.1 to 0.5 (Walder and Hallet (1979) measured 0.2 for Blackfoot Glacier). The added pressure on the bed would be $\Delta p = \Delta p_c a_c$, averaged over an area of the bed containing many bumps and cavities. Within the assumed range of a_c, the total pressure change would be 0.02 to 0.1 MPa. For crystalline bedrock with a Young's modulus E of 50 GPa (Turcotte and Schubert, 2002), and assuming uniaxial strain due to a uniformly distributed surface load, deformation of a $h = 5$m thick column of rock between the glacier bed and the tunnel floor would be $\Delta z = h\Delta p/E$, or as large as 0.01 mm. Indeed, the presence of a void

in the rock (i.e., the research tunnel) could locally enhance the deformation under the added water pressure load, leading to larger and more complex deformations than calculated by this simplistic analysis.

While we do not have sufficient information to undertake a rigorous analysis of the deformation of the subglacial rock, a tilt angle of 5 μrad (e.g., Fig DR4, DR7-9) would accompany rigid rotation by 0.05 mm of a member of characteristic length of l = 10 m, which is a small but reasonable length scale for a water pressure disturbance and is approximately the length of the shaft area of the research tunnel (Fig. DR1B).

4. References

Burtin, A., Bollinger, L., Vergne, J., Cattin, R., and Nábělek, J.L., 2008, Spectral analysis of seismic noise induced by rivers: A new tool to monitor spatiotemporal changes in stream hydrodynamics: Journal of Geophysical Research, v. 113, no. B5, p. 1–14, doi: 10.1029/2007JB005034.

Cohen, D., Hooyer, T.S., Iverson, N.R., Thomason, J.F., and Jackson, M., 2006, Role of transient water pressure in quarrying: A subglacial experiment using acoustic emissions: Journal of Geophysical Research, v. 111, no. F3, p. F03006, doi: 10.1029/2005JF000439.

Cohen, D., Iverson, N.R., Hooyer, T.S., Fischer, U.H., Jackson, M., and Moore, P.L., 2005, Debris-bed friction of hard-bedded glaciers: Journal of Geophysical Research, v. 110, no. F2, p. 1–15, doi: 10.1029/2004JF000228.

Genco, R., and Ripepe, M., 2010, Inflation-deflation cycles revealed by tilt and seismic records at Stromboli volcano: Geophysical Research Letters, v. 37, no. 12, doi: 10.1029/2010GL042925.

Iverson, N.R., Cohen, D., Hooyer, T.S., Fischer, U.H., Jackson, M., Moore, P.L., Lappegard, G., and Kohler, J., 2003, Effects of basal debris on glacier flow.: Science (New York, N.Y.), v. 301, no. 5629, p. 81–4, doi: 10.1126/science.1083086.

Iverson, N.R., Hooyer, T.S., Fischer, U.H., Cohen, D., Moore, P.L., Jackson, M., Lappegard, G., and Kohler, J., 2007, Soft-bed experiments beneath Engabreen, Norway: regelation infiltration, basal slip and bed deformation: Journal of Glaciology, v. 53, no. 182, p. 323–340, doi: 10.3189/002214307783258431.

Jackson, M., Brown, I.A., and Elvehøy, H., 2005, Velocity measurements on Engabreen , Norway: Annals of Glaciology, v. 42, no. 1, p. 29–34.

Lappegard, G., and Kohler, J., 2005, Determination of basal hydraulic systems based on subglacial high-pressure pump experiments: Annals of Glaciology, v. 40, no. 1, p. 37–42, doi: 10.3189/172756405781813681.

Lappegard, G., Kohler, J., Jackson, M., and Hagen, J.O., 2006, Characteristics of subglacial drainage systems deduced from load-cell measurements: Journal of Glaciology, v. 52, no. 176, p. 137–148, doi: 10.3189/172756506781828908.

Turcotte, D., and Schubert, G., 2002, Geodynamics:.

Walder, J., and Hallet, B., 1979, Geometry of former subglacial water channels and cavities: Journal of Glaciology, v. 23, no. 89, p. 335–346.

Wielandt, E., and Forbriger, T., 1999, Near-field seismic displacement and tilt associated with the explosive activity of Stromboli: Annali di Geofisica, v. 42, no. 3, p. 407–416.

Wiens, D., Pozgay, S., Shore, P., Sauter, A., and White, R., 2005, Tilt recorded by a portable broadband seismograph: The 2003 eruption of Anatahan Volcano, Mariana Islands: Geophysical Research Letters, v. 32, no. 18, p. L18305, doi: 10.1029/2005GL023369.

DR FIGURES & CAPTIONS

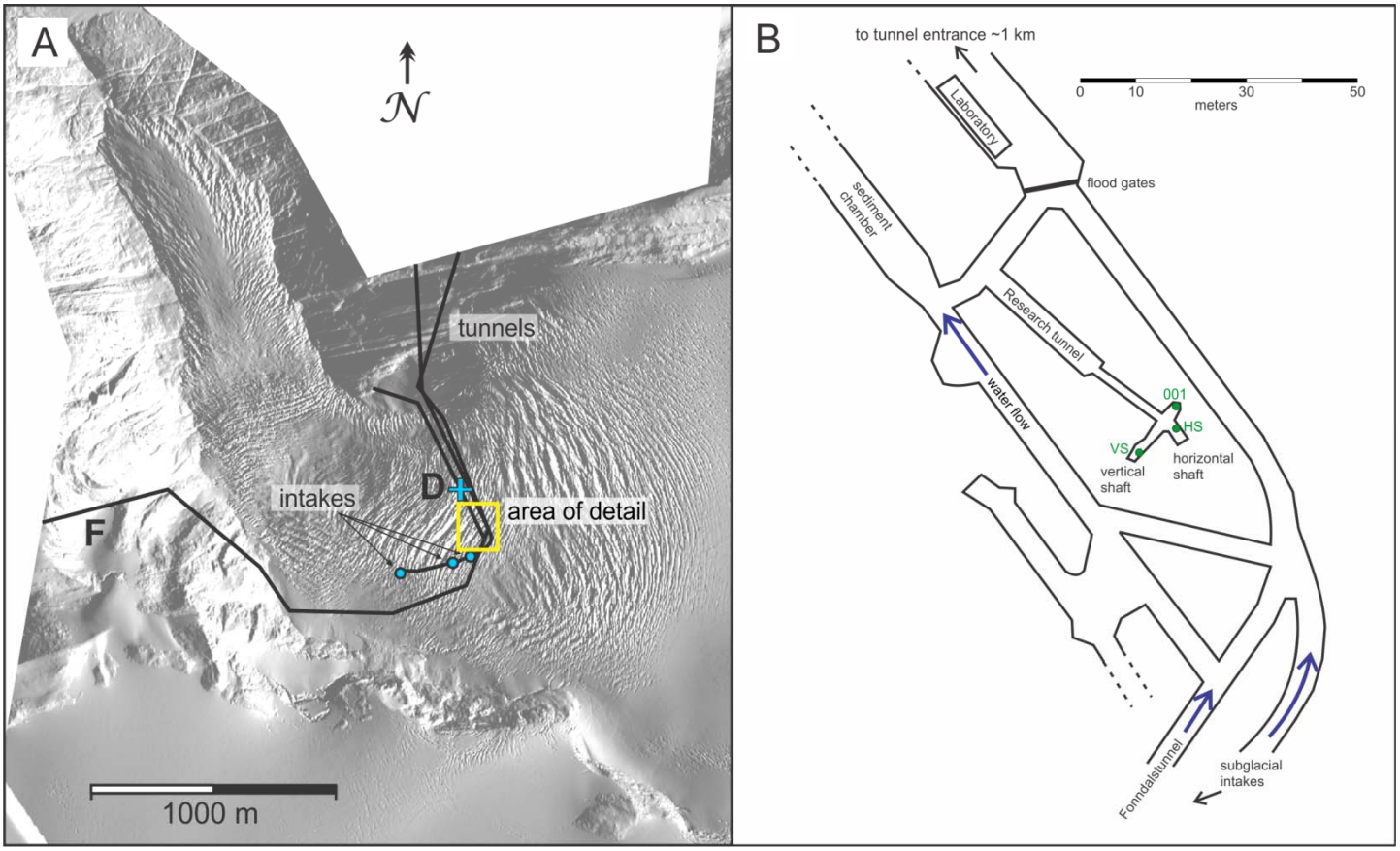

FIG DR1. Maps of the Engabreen subglacial tunnel system. **A.** Schematic layout of the tunnel system superimposed on a shaded relief map derived from airborne laser altimetry (as in Fig. 1). The tunnel marked F denotes Fonndalstunnelen, which captures subaerial snow and ice melt in a valley west of Engabreen. Three blue circles marked "intakes" capture water draining along the glacier bed. The blue cross marked "D" indicates the approximate location of the gaging station at the downstream end of the sediment chamber. An additional gaging station measures flow above the junction of Fonndalstunnelen with the tunnel draining the subglacial intakes. The yellow box shows the area detailed in panel B. **B.** Schematic tunnel layout in the area of the subglacial research tunnel and the subglacial laboratory. Access to the glacier bed is through the horizontal and vertical shafts in the southeast end of the research tunnel. Green circles near the shafts denote the locations of broadband seismometers installed during 2010 and 2011.

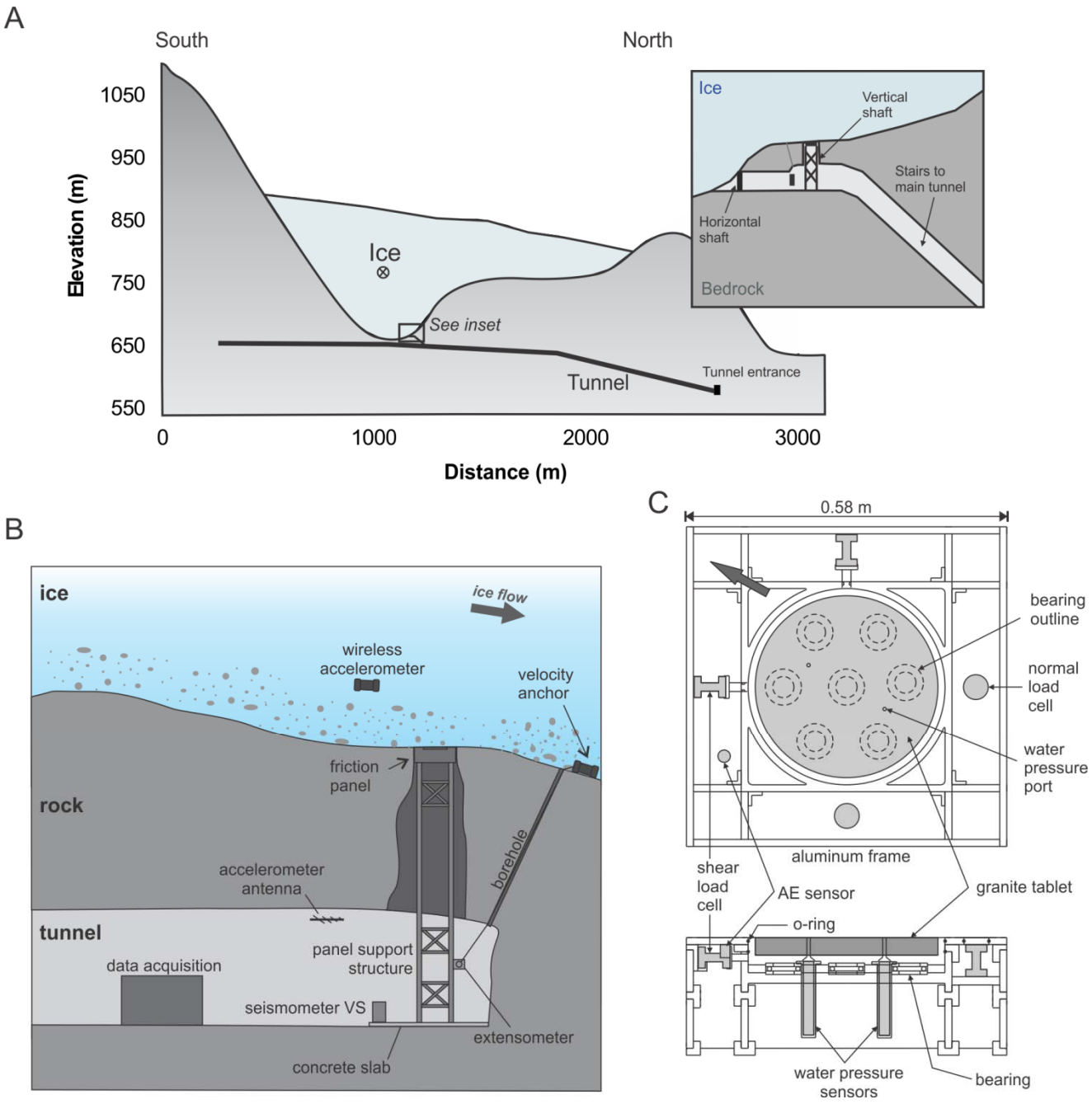

Fig. DR2. Schematic diagrams of the subglacial access points and research instrumentation used in the vertical shaft area. **A.** Schematic north-south cross-section across Engabreen in the vicinity of the subglacial accesses. Inset shows an enlargement of the upper part of the research tunnel (floor-to ceiling tunnel height is approximately 3m) **B.** Schematic layout of subglacial instrumentation near the vertical shaft. See supplementary text for descriptions of each instrument. Floor-to-ceiling height of the tunnel is approximately 3m. **C.** Dimensional drawings showing the key components of the friction panel. The upper drawing is a map-view and the lower drawing is a cross-section parallel to an edge of the panel

but oblique to ice flow. Components described in the supplementary text are shown in gray. The dark gray arrow in the upper left indicates the local ice flow direction as inferred from striations in the bedrock.

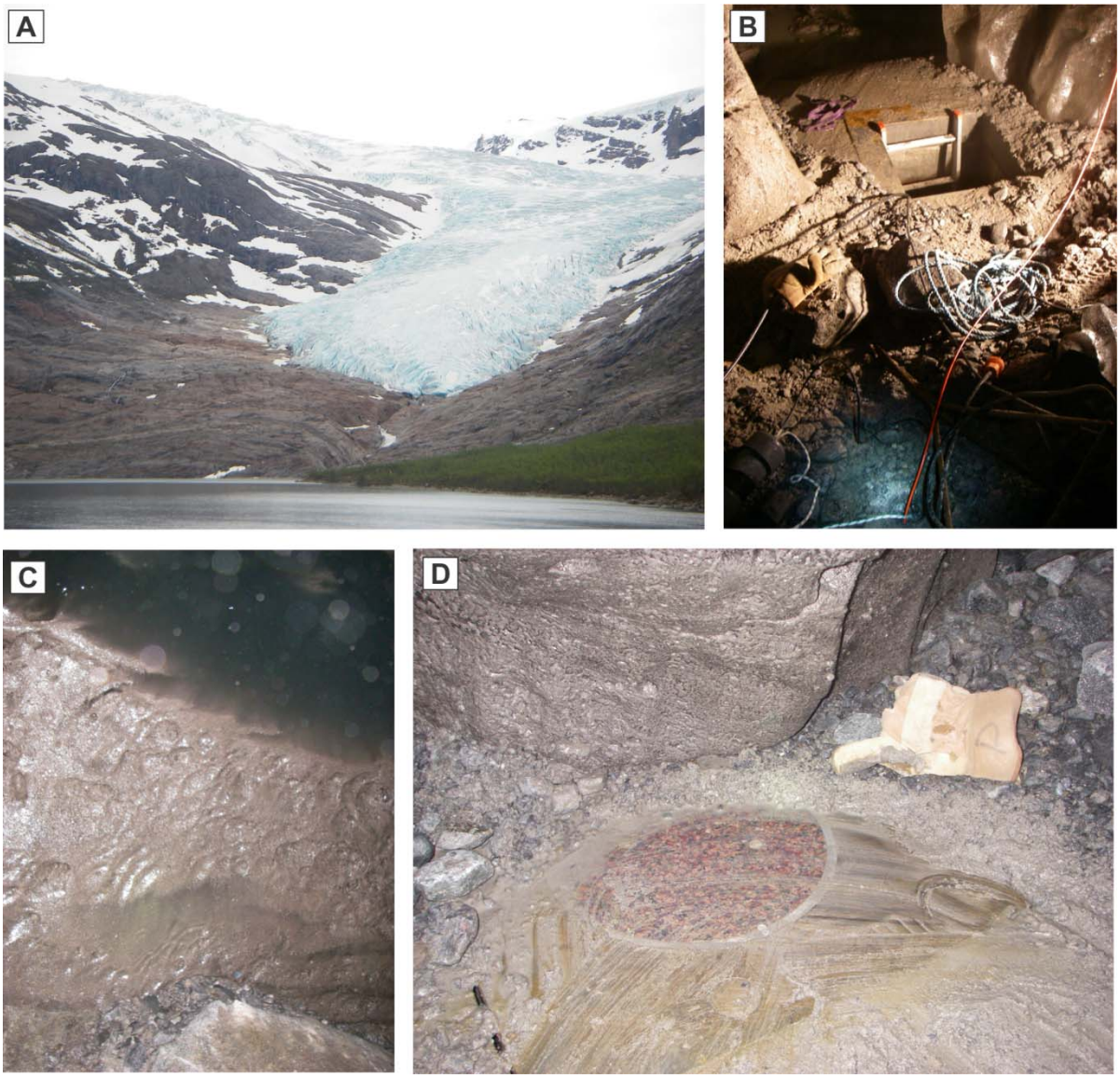

Fig. DR3. Photos of Engabreen and the the ice-bed interface. **A.** Engabreen's terminus from the north taken in May 2011. **B.** The vertical shaft opening (0.58 m across) from above, taken from inside a cavity melted into basal ice. A gray smart-rock enclosure is shown in the lower left corner. Striations on the bedrock in the upper part of the photo indicate the local ice-flow direction into the page. **C.** Close-up of debris-bearing basal ice (brown band in the center) beneath clear ice and resting on bedrock (the light brown area visible in the lower middle and lower right of the photo). A thin, unfrozen gravelly sediment layer appears to separate the dirty basal ice from the rock beneath in some places. The field of view is approximately 0.5m from top to bottom. **D.** Ice encroaching on the friction panel 24 hours after installation. The 0.3m diameter pink granite tablet is ~30% covered with basal ice and gravelly sand that was melted out of the ice. The finger on the glove is pointing in the flow direction. Photo taken on May 6, 2011.

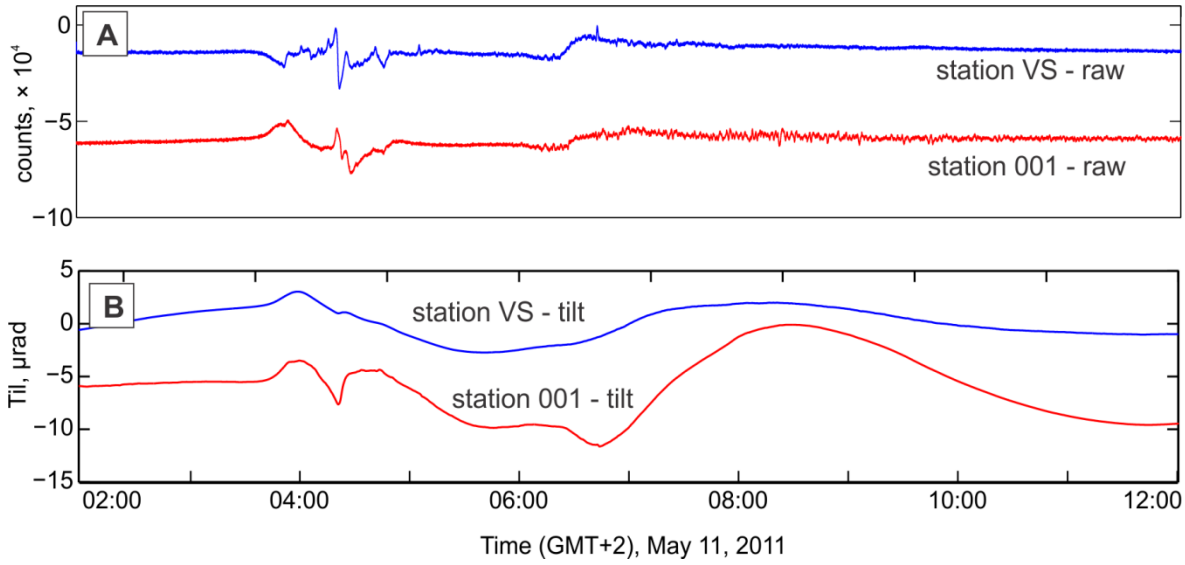

Fig. DR4. Comparison of the May 11, 2011 meltwater event as measured in two broadband seismometers located on opposite ends of the access area in the research tunnel. **A.** Raw E-W component of seismicity for stations VS ad 001 in the research tunnel, low-pass filtered below 1 Hz and expressed in digital counts. See Fig. DR1 for seismometer locations. **B.** ULP seismometer-derived tilt angle, from the same components of the broadband seismometers shown in A, band-pass filtered from 100-35,000 seconds.

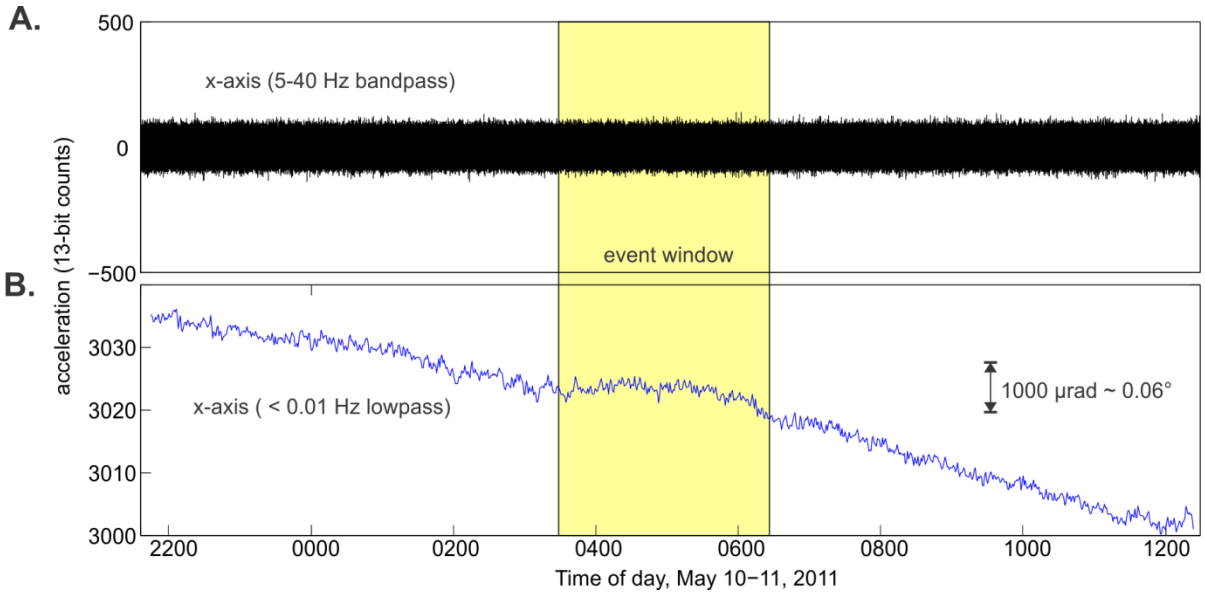

Fig. DR5. Wireless accelerometer data from a single axis of a "smart rock" embedded in the basal ice, 1.0 m above the glacier bed near the friction panel, during late night May 10 and the morning of May 11, 2011. **A.** Bandpass-filtered (5-40 Hz, 5-pole Butterworth) x-axis acceleration. **B.** Low-pass filtered (< 0.01 Hz) data from the same axis showing interruption of a transient bias shift during the same time that other subglacial measurements (shown in Fig. 3 in the main text) indicate disturbances in stress, water pressure and the character of sliding (indicated by the yellow box labeled "event window"). At the time of installation in the basal ice, the x-axis was oriented approximately NW-SE.

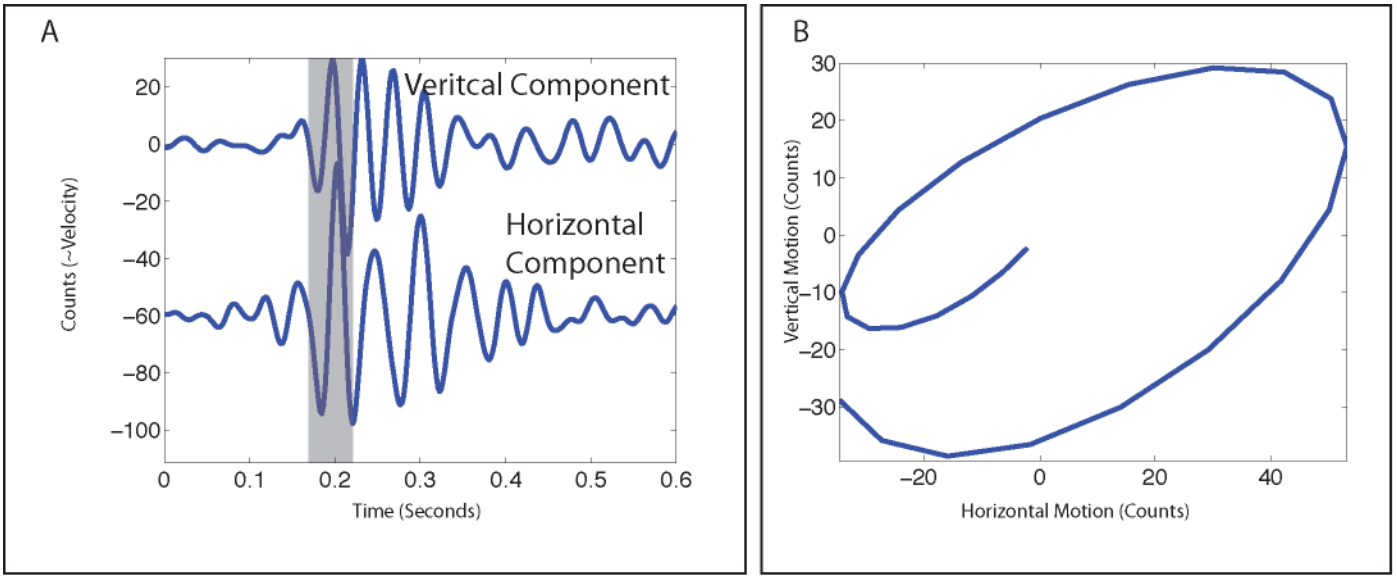

Fig. DR6. Example icequake recorded by seismometer 001 in the research shaft. **A.** Vertical and horizontal components of motion for a typical icequake with a 5-30 Hz bandpass filter applied. **B.** Particle motion plot for shaded region in A, showing retrograde motion typical of Rayleigh waves and indicating shallow origin.

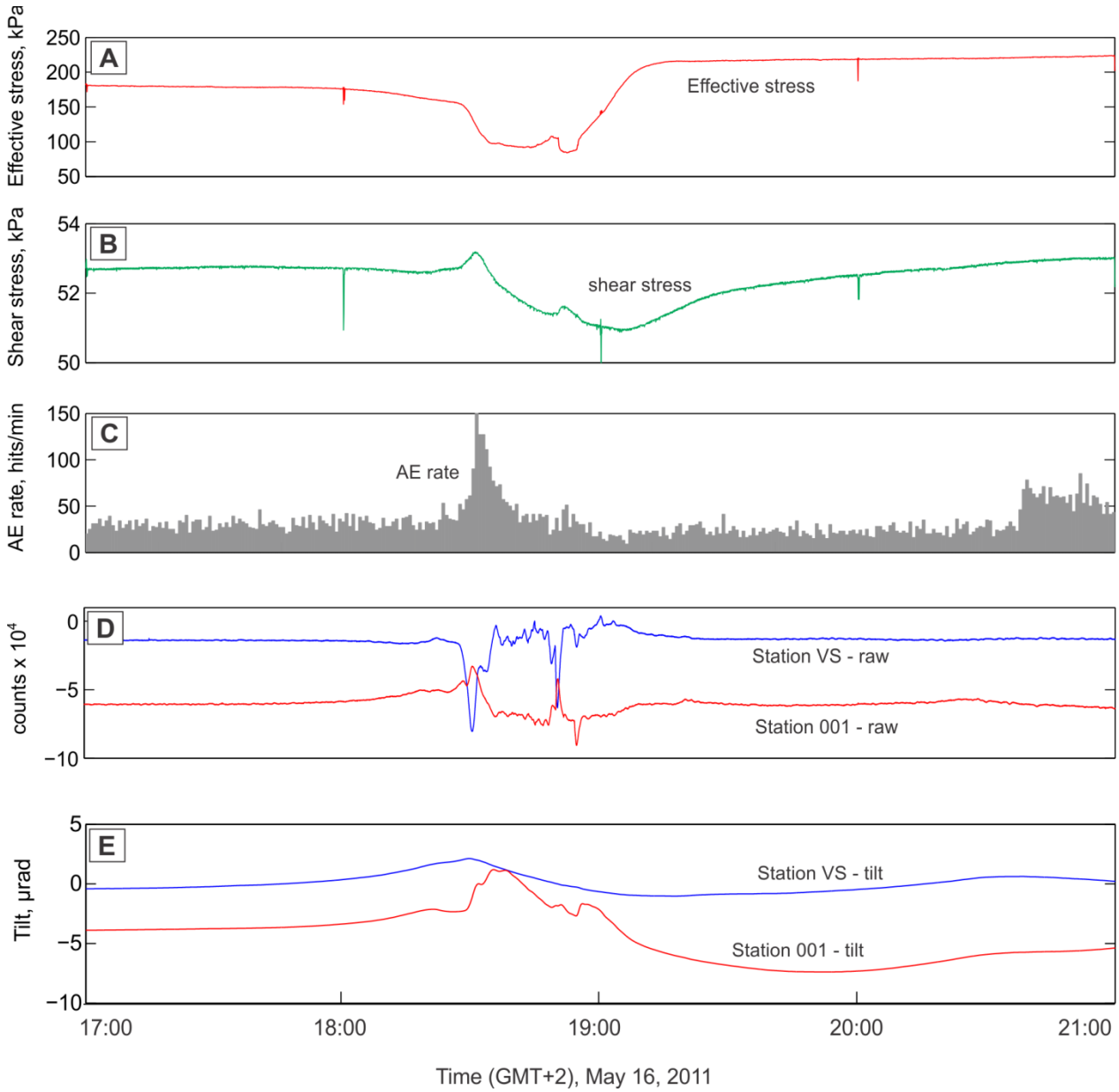

Fig. DR7. Meltwater event of May 16, 2011 as recorded in the friction panel and broadband seismometers. **A.** Basal effective stress on the panel; **B.** Shear stress on the panel. **C.** Acoustic emissions rate from the friction panel. **D.** Raw E-W component of seismicity for stations VS and 001 in the research tunnel, low-pass filtered below 1 Hz and expressed in digital counts. See Fig. DR1 for seismometer locations. **E.** ULP seismometer-derived tilt angle from the same components of the broadband seismometers shown in D, band-pass filtered from 100-35,000 s.

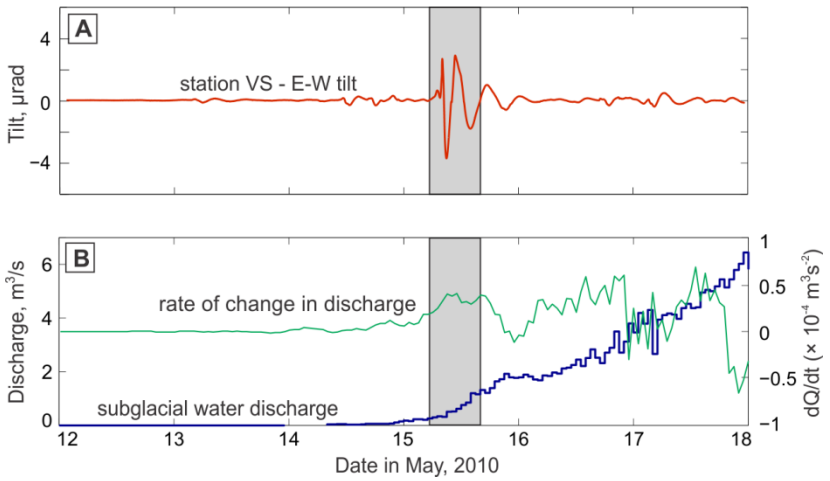

Fig. DR8. Long-period tilt and subglacial discharge from May 12-18, 2010. The gray shading encloses the May 15 event discussed in the text and shown in Fig. DR9. **A.** Tilt magnitude derived from long-period seismic record in the E-W component of broadband seismometer at station VS. **B.** Subglacial component of water discharge through the collection tunnels (blue) and its time derivative (green). The time derivative was computed numerically by forward differencing after applying a 5-point (2 hour) moving average filter the discharge data.

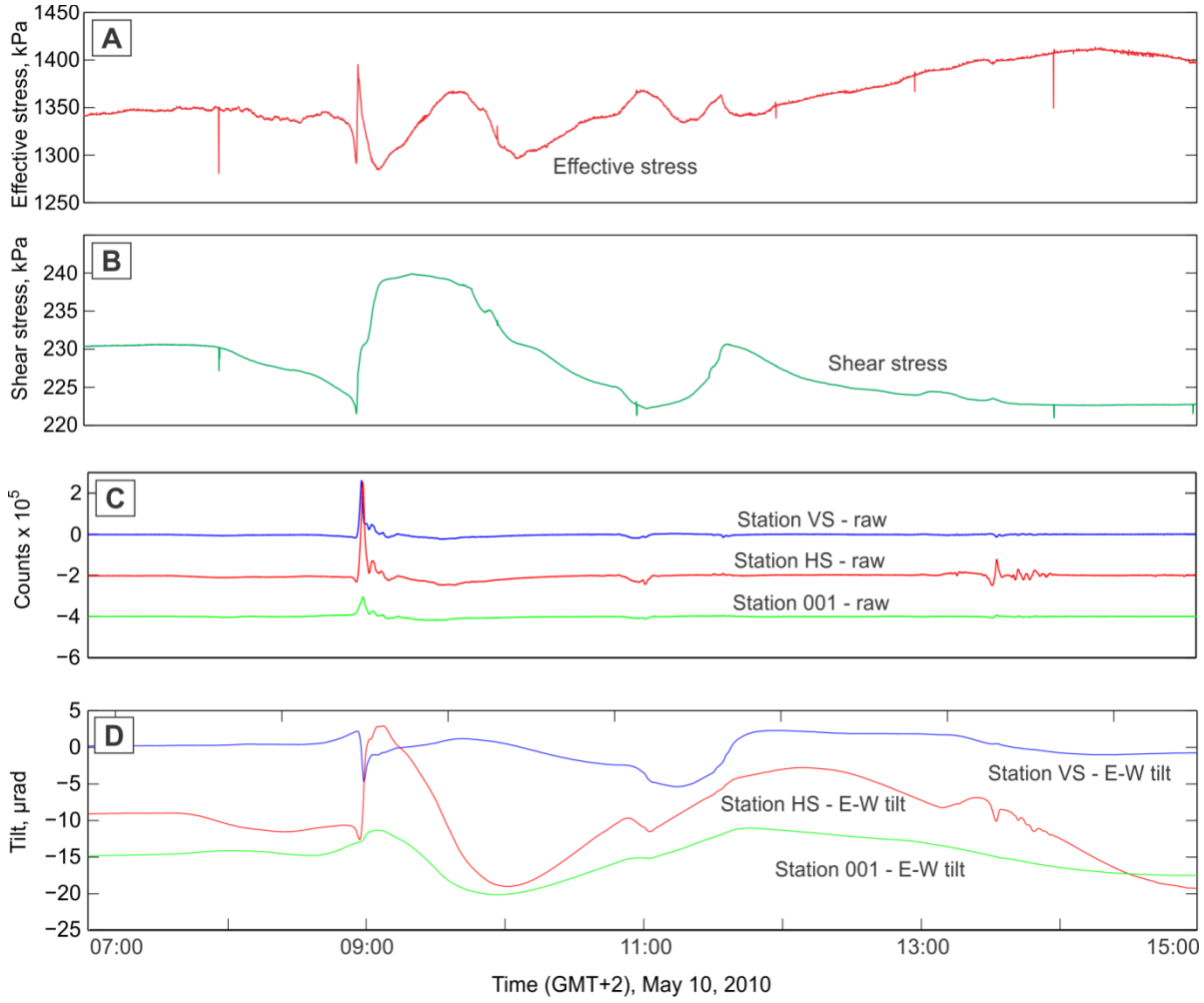

Fig. DR9. Meltwater event of May 15, 2010, as recorded in the friction panel and broadband seismometers. **A.** Basal effective stress on the panel. **B.** Shear stress on the panel (a minimum value since only one of two load cells was working at the time). **C.** Raw E-W component of seismicity for stations VS, HS, and 001 in the research tunnel, low-pass filtered below 1 Hz and expressed in digital counts. See Fig. DR1 for seismometer locations. **D.** Tilt magnitude derived from the same components of the broadband seismometers shown in C, band-pass filtered from 100-35,000 s.